Intraindividual Comparison of ^{18}F-PSMA-1007 and ^{18}F-DCFPyL PET/CT in the Prospective Evaluation of Patients with Newly Diagnosed Prostate Carcinoma: A Pilot Study

Frederik L. Giesel*[1,2], Leon Will*[1], Ismaheel Lawal[3], Thabo Lengana[3], Clemens Kratochwil[1], Mariza Vorster[3], Oliver Neels[4], Florette Reyneke[3], Uwe Haberkon[1,2], Klaus Kopka[4], and Mike Sathekge[3]

[1]Department of Nuclear Medicine, Heidelberg University Hospital, Heidelberg, Germany; [2]Cooperation Unit Nuclear Medicine, German Cancer Research Center, Heidelberg, Germany; [3]Department of Nuclear Medicine, University of Pretoria and Steve Biko Academic Hospital, Pretoria, South Africa; and [4]Division of Radiopharmaceutical Chemistry, German Cancer Research Center, Heidelberg, Germany

The introduction of ^{18}F-labeled prostate-specific membrane antigen (PSMA)–targeted PET/CT tracers, first ^{18}F-DCFPyL (2-(3-{1-carboxy-5-[(6-^{18}F-fluoro-pyridine-3-carbonyl)-amino]-pentyl}-ureido)-pentanedioic acid) and more recently ^{18}F-PSMA-1007 (((3*S*,10*S*,14*S*)-1-(4-(((*S*)-4-carboxy-2-((*S*)-4-carboxy-2-(6-^{18}F-fluoronicotinamido)butanamido)butanamido)methyl)phenyl)-3-(naphthalen-2-ylmethyl)-1,4,12-trioxo-2,5,11,13-tetraazahexadecane-10,14,16-tricarboxylic acid)), have demonstrated promising results for the diagnostic workup of prostate cancer. This clinical study presents an intraindividual comparison to evaluate tracer-specific characteristics of ^{18}F-DCFPyL versus ^{18}F-PSMA-1007. **Methods:** Twelve prostate cancer patients, drug-naïve or before surgery, received similar activities of about 250 MBq of ^{18}F-DCFPyL and ^{18}F-PSMA-1007 48 h apart and were imaged 2 h after injection on the same PET/CT scanner using the same reconstruction algorithm. Normal-organ biodistribution and tumor uptake were quantified using SUV_{max}. **Results:** PSMA-positive lesions were detected in 12 of 12 prostate cancer patients. Both tracers, ^{18}F-DCFPyL and ^{18}F-PSMA-1007, detected the same lesions. No statistical significance could be observed when comparing the SUV_{max} of ^{18}F-DCFPyL and ^{18}F-PSMA-1007 for local tumor, lymph node metastases, and bone metastases. With regard to normal organs, ^{18}F-DCFPyL had statistically significant higher uptake in kidneys, urinary bladder, and lacrimal gland. Vice versa, significantly higher uptake of ^{18}F-PSMA-1007 in muscle, submandibular and sublingual gland, spleen, pancreas, liver, and gallbladder was observed. **Conclusion:** Excellent imaging quality was achieved with both ^{18}F-DCFPyL and ^{18}F-PSMA-1007, resulting in identical clinical findings for the evaluated routine situations. Nonurinary excretion of ^{18}F-PSMA-1007 might present some advantage with regard to delineation of local recurrence or pelvic lymph node metastasis in selected patients; the lower hepatic background might favor ^{18}F-DCFPyL in late stages, when rare cases of liver metastases can occur.

Key Words: ^{18}F-PSMA-1007; ^{18}F-DCFPyL; prostate carcinoma; PET/CT; PSMA

J Nucl Med 2018; 59:1076–1080
DOI: 10.2967/jnumed.117.204669

Prostate-specific membrane antigen (PSMA)–targeted PET/CT is a relatively new technique for imaging prostate cancer. Initial results in the evaluation of various clinical indications, such as imaging-guided biopsy, primary tumor staging, localization of biochemical relapse, planning of radiotherapy, and prediction and assessment of tumor response to systemic therapy are promising and have been summarized in detail recently (*1–4*). Currently, most clinical experience is with the ligand Glu-urea-Lys(Ahx)-HBED-CC (HBED-CC is *N,N′*-bis[2-hydroxy-5-(carboxyethyl) benzyl]ethylenediamine-*N,N′*-diacetic acid) labeled with the generator radionuclide ^{68}Ga (^{68}Ga-PSMA-11). However, because of the promising clinical results, it is predictable that the request for PSMA-PET/CT examinations will increase, and this foreseeable demand has promoted the development of ^{18}F-labeled ligands using ^{18}F-fluoride, a radionuclide that can be produced and distributed in large scale and at reasonable cost by a cyclotron.

After preclinical evaluation of several ^{18}F-labeled PSMA ligands, ^{18}F-DCFPyL (2-(3-{1-carboxy-5-[(6-^{18}F-fluoro-pyridine-3-carbonyl)-amino]-pentyl}-ureido)-pentanedioic acid) and ^{18}F-PSMA-1007 (((3*S*,10*S*,14*S*)-1-(4-(((*S*)-4-carboxy-2-((*S*)-4-carboxy-2-(6-^{18}F-fluoronicotinamido)butanamido)butanamido)methyl)phenyl)-3-(naphthalen-2-ylmethyl)-1,4,12-trioxo-2,5,11,13-tetraazahexadecane-10,14,16-tricarboxylic acid)) were considered the most promising candidates (*5,6*) and have recently been introduced clinically (*7,8*). ^{18}F-DCFPyL has already demonstrated noninferiority versus ^{68}Ga-PSMA-11 in a one-on-one evaluation of 25 patients (*9*). Another 62 patients examined with ^{18}F-DCFPyL were found noninferior to historical controls examined with ^{68}Ga-PSMA-11 in a similar clinical indication (*9*). Before now, ^{18}F-PSMA-1007 had not yet been benchmarked against other PSMA ligands. In this study, an intraindividual comparison of ^{18}F-DCFPyL and ^{18}F-PSMA-1007 was performed.

MATERIALS AND METHODS

Patients

Twelve patients (median age, 66 y; range, 54–82 y) with newly diagnosed, treatment-naïve prostate cancer were included in this study, which was approved by the Institutional Ethics Committee (University of Pretoria, South Africa). Written informed consent was obtained from all patients. The patient characteristics are detailed in Table 1.

Radiopharmaceuticals

The radiolabeling precursors were obtained in good-manufacturing-practice grade by ABX Advanced Biochemical Compounds.

Received Nov. 6, 2017; revision accepted Nov. 28, 2017.
For correspondence or reprints contact: Mike Sathekge, Department of Nuclear Medicine, University of Pretoria and Steve Biko Academic Hospital, Private Bag X169, Pretoria, 0001, South Africa.
E-mail: mike.sathekge@up.ac.za
*Contributed equally to this work.
Published online Dec. 21, 2017.

TABLE 1
Patient Characteristics

Patient no.	Age (y)	Gleason score	PSA at examination (ng/mL)	Local tumor growth (*n*)	Lymph node metastases (*n*)	Bone metastases (*n*)
1	54	9 (4 + 5)	124.0	1	>10	>10
2	55	8 (4 + 4)	112.0	1	0	0
3	60	6 (3 + 3)	13.4	1	0	0
4	66	8 (4 + 4)	75.0	1	>10	4
5	80	8 (4 + 4)	95.4	1	0	0
6	82	9 (5 + 4)	240.0	1	>10	>10
7	66	7b (4 + 3)	87.0	3	0	0
8	66	7a (3 + 4)	61.6	1	0	0
9	69	7a (3 + 4)	10.0	2	0	0
10	62	7b (4 + 3)	83.0	1	1	0
11	79	8 (4 + 4)	279.8	1	>10	0
12	65	7a (3 + 4)	55.2	1	0	0

^{18}F-PSMA-1007 was produced on an automated radiosynthesizer (Tracerlab FX F-N; GE Healthcare) in a single-step radiosynthesis (*10*) followed by simple solid-phase extraction of the product by cartridge separation. The synthesis of ^{18}F-DCFPyL was performed as reported by Chen et al. (*5*). Analysis and quality control of the prepared products were as previously reported (*8*).

Imaging Procedures

Imaging was performed on 2 different days to minimize the effects of possible competitive interactions of the radiotracers. The first 6 patients were imaged with ^{18}F-DCFPyL and then 48 h later with ^{18}F-PSMA-1007. The next 6 patients were examined with ^{18}F-PSMA-1007 and then 48 h later with ^{18}F-DCFPyL. The patients fasted for at least 4 h before injection of the radiotracer. For both tracers, the injected activities were 240–260 MBq and imaging began 2 h after injection.

All scans were obtained on a Biograph mCT 40 PET/CT scanner (Siemens). For both tracers, an unenhanced CT scan was obtained, followed by PET scans from thighs to vertex. CT parameters were adjusted for patient weight (120 keV, 40–150 mAs), with a section width of 5 mm and a pitch of 0.8. Vertex to mid-thigh PET imaging was performed in 3-dimensional mode at 3 min per bed position. CT data were used for attenuation correction. Images were reconstructed with an ordered-subset expectation-maximization iterative reconstruction algorithm (4 iterations, 8 subsets). A gaussian filter of 5.0 mm in full width at half maximum was applied.

Image Analysis and Quantification

Clinical images were interpreted independently by 2 board-certified nuclear medicine physicians, who did not disagree on any of the interpretations. The readers were masked to the findings on complementary imaging.

The tracer biodistribution was quantified by SUV_{max}. Reconstructed images were displayed on a dedicated workstation equipped with Syngo software (Siemens). A semiautomatic spheric volume of interest was drawn around lesions using an SUV threshold of 2.5 and a 3-dimensional isocontour of 41%. The volume of interest was manually adjusted to exclude areas of intense physiologic uptake contiguous to tumor. All primary tumors and up to 5 lymph nodes and 5 bone metastases, chosen by chance, were quantified. The normal bladder, background, brain, salivary and lacrimal glands, lung, liver, spleen, pancreas, small intestine, and kidneys were evaluated with a 2-cm sphere placed inside the organ parenchyma.

Statistical Analysis

Statistical analysis was performed using SPSS software, version 24.0 (IBM Corp.). For comparison of uptake values, the nonparametric Wilcoxon signed-rank test for 2 related samples was used. The significance level used was a P value of 0.05 or less (2-tailed).

RESULTS

All subjects tolerated the examinations well, and no drug-related adverse events occurred. The patients did not report any subjective symptoms. With regard to the clinical imaging interpretation, both readers were concordant.

PSMA tracer–positive lesions were found in all patients. All lesions detected by ^{18}F-PSMA-1007 PET/CT were also detected by ^{18}F-DCFPyL PET/CT and vice versa. Seven patients presented with solitary tracer uptake in the prostate (Figs. 1 and 2). One

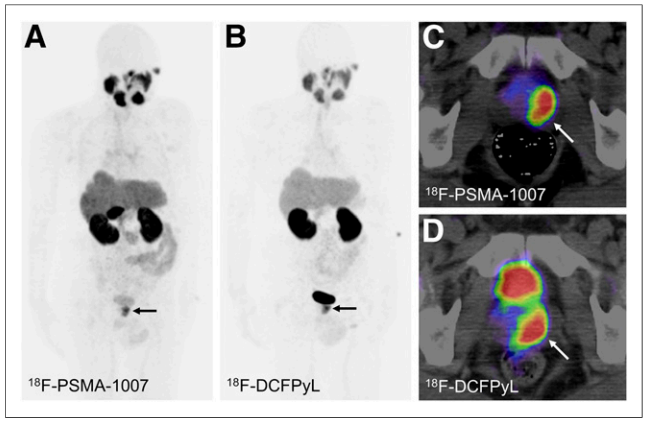

FIGURE 1. PET/CT images of 80-y-old patient with newly diagnosed prostate cancer referred because of PSA serum level of 95.43 ng/mL and positive biopsy (Gleason score 8 [4 + 4]). Patient was examined with ^{18}F-DCFPyL (B and D) in May 2017. Second examination with ^{18}F-PSMA-1007 followed 48 h later (A and C). Diagnosis of prostate cancer confined to prostate gland (arrows) was possible with both tracers. SUV_{max} in this lesion was 18.08 and 11.77 for ^{18}F-DCFPyL and ^{18}F-PSMA-1007, respectively.

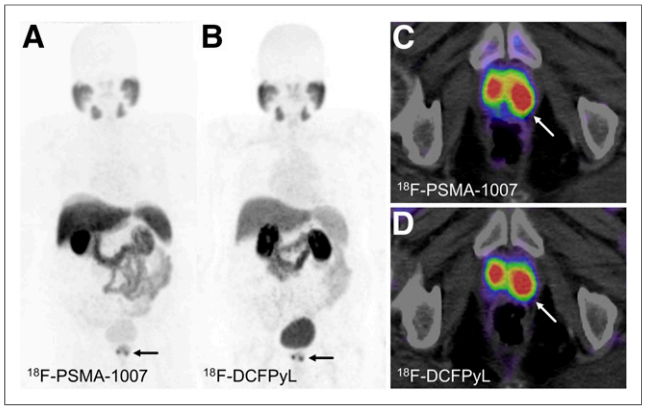

FIGURE 2. PET/CT images of 65-y-old patient referred because of Gleason score of 7a (3 + 4) and PSA serum level of 55.2 ng/mL. Patient was examined with ^{18}F-PSMA-1007 (A and C) and ^{18}F-DCFPyL (B and D). Images showed bifocal prostate cancer (arrows). Delineation of tumor growth in both lobes of prostate was possible with both tracers. SUV_{max} was 17.68 and 19.65 in right lobe and 14.21 and 16.60 in left lobe for ^{18}F-DCFPyL and ^{18}F-PSMA-1007, respectively.

patient was diagnosed with prostate cancer and a single lymph node metastasis in the pelvis. In 4 patients, advanced metastatic disease was detected (Fig. 3).

Tumor Uptake

No statistically significant difference was found when evaluating uptake of ^{18}F-PSMA-1007 and ^{18}F-DCFPyL for local tumor growth (median SUV_{max}, 17.65 vs. 18.08; $P = 0.175$; $n = 12$), lymph node metastases (median SUV_{max}, 13.97 vs. 17.33; $P = 0.109$; $n = 17$), and bone metastases (median SUV_{max}, 10.19 vs. 11.63; $P = 0.153$; $n = 15$). Detailed uptake characteristics for each lesion group are shown in Figure 4.

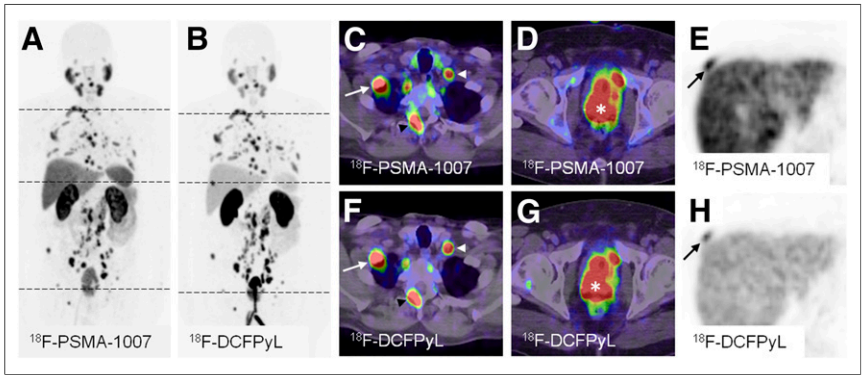

FIGURE 3. Maximum-intensity projections of PET examinations using ^{18}F-PSMA-1007 (A) and ^{18}F-DCFPyL (B), as well as exemplary PET/CT and CT cross-sections with bone and lymph node metastases (C, E, F, and H) and local tumor (D and G). The 82-y-old patient presented with PSA serum level of 240.0 ng/mL at time of examinations. Subject was diagnosed with highly advanced metastatic prostate cancer (Gleason 9 [5 + 4]) and was treatment-naïve at the time of the examinations. The SUV_{max} values were 22.80 and 19.69 in the prostate (D, G, asterisk), 16.50 and 11.20 in an exemplary lymph node (C, F, white arrowhead), and 16.20 and 13.72 (C, F, white arrow) and 25.45 and 24.90 (A, D) in exemplary bone lesions for ^{18}F-DCFPyL and ^{18}F-PSMA-1007, respectively. The maximum-intensity projections (A, B) demonstrate a bone lesion that could be missed on the ^{18}F-PSMA-1007 maximum-intensity projection (A). However, it is delineable on transaxial cross-sections (E, H, black arrow). This lesion presents with SUV_{max} values of 23.72 and 17.97 for ^{18}F-DCFPyL and ^{18}F-PSMA-1007, respectively. This case highlights differences in biodistribution of tracers and similar uptake in all tumor lesions. A urinary catheter is also seen.

Normal-Organ Uptake

The biodistribution of the two tracers differed, as ^{18}F-DCFPyL had renal clearance and ^{18}F-PSMA-1007 had hepatobiliary clearance. Uptake was significantly higher for ^{18}F-DCFPyL than for ^{18}F-PSMA-1007 in the kidneys (median SUV_{max}, 37.50 vs. 22.08; $P < 0.001$), urinary bladder (median SUV_{max}, 79.32 vs. 9.32; $P < 0.001$), and lacrimal gland (median SUV_{max}, 8.37 vs. 7.30; $P = 0.036$), whereas ^{18}F-PSMA-1007 showed significantly higher uptake in the liver (median SUV_{max}, 16.94 vs. 9.07; $P < 0.001$), gallbladder (median SUV_{max}, 53.04 vs. 6.15; $P = 0.001$), spleen (median SUV_{max}, 14.32 vs. 6.68; $P < 0.001$), pancreas (median SUV_{max}, 4.55 vs. 2.95; $P = 0.003$), submandibular gland (median SUV_{max}, 17.39 vs. 13.20; $P = 0.011$), sublingual gland (median SUV_{max}, 3.97 vs. 3.30; $P = 0.006$), and muscle (median SUV_{max}, 1.10 vs. 0.97; $P = 0.034$). Uptake did not differ significantly in fat tissue, blood pool (thoracic aorta), brain, nasal mucosa, parotid gland, lung, or small intestine. A detailed comparison is shown in Figure 4.

DISCUSSION

In this intraindividual comparison of patients with treatment-naïve prostate cancer, the diagnostic performance and tumor targeting of ^{18}F-DCFPyL and ^{18}F-PSMA-1007 were nearly identical. ^{18}F-DCFPyL was predominantly eliminated by renal clearance into the urinary bladder, whereas ^{18}F-PSMA-1007 showed hepatobiliary excretion characteristics.

Addressing the identical target structure, it is no surprise that all PSMA diagnostic agents, including the ^{68}Ga- (*11*) or ^{99m}Tc-labeled (*12*) compounds, have a similar specific accumulation in tumor and physiologic PSMA-expressing normal organs such as the healthy prostate, kidney parenchyma, salivary glands, and small intestine. ^{18}F-DCFPyL and ^{18}F-PSMA-1007 belong to the same family of PSMA ligands based on the Glu-urea-Lys motif targeting the catalytic domain of PSMA and also share an aromatic portion considered to exploit the S1 hydrophobic accessory pocket close to the enzymatic binding site or the arene binding site (*13*). Both tracers use the same radiolabel, ^{18}F, which, on the basis of its nuclear physical properties should allow a spatial resolution equal to or even better than that of ^{68}Ga (*14*). Thus, comparable tumor targeting properties of these two evaluated ^{18}F-labeled tracers are reasonable and well addressed. In contrast, some differences can occur in the excretory organs. Vallabhajosula et al. already observed that structurally similar PSMA ligands can differ concerning hepatic (MIP-1404) or urinary (MIP-1405) excretion (*12*) and that, because of rare hepatic metastases in prostate cancer, the MIP-1404 tracer with the lower bladder activity was chosen for phase 2 and 3 clinical trials (NCT0261506) (*15*). Because local relapses are common and simultaneously a diagnostic challenge in the work-up of biochemical recurrence, this rationale might also account for the ^{18}F-PSMA-1007 imaging findings.

Molecular size and excretion kinetics may also affect the velocity of tumor targeting

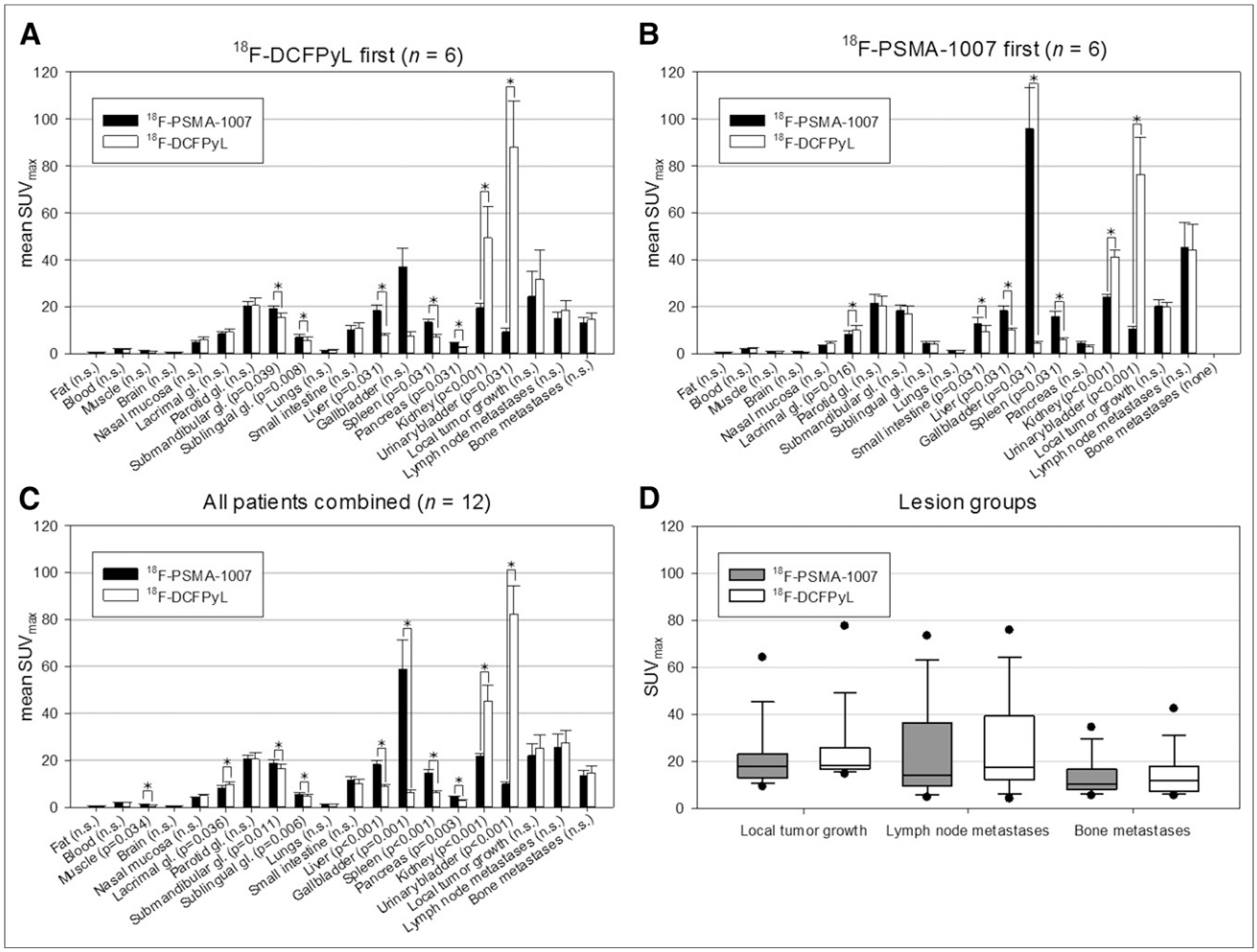

FIGURE 4. (A) Comparison of mean SUV_{max} and its SE 2 h after injection of ^{18}F-PSMA-1007 and ^{18}F-DCFPyL for normal organs and tumors in 6 patients examined with ^{18}F-DCFPyL before being examined with ^{18}F-PSMA-1007. (B) Comparison of mean SUV_{max} and its SE 2 h after injection of ^{18}F-PSMA-1007 and ^{18}F-DCFPyL for normal organs and tumors in 6 patients examined with ^{18}F-PSMA-1007 before being examined with ^{18}F-DCFPyL. (C) Comparison of mean SUV_{max} and its SE 2 h after injection of ^{18}F-PSMA-1007 and ^{18}F-DCFPyL for normal organs and tumors in all patients. (D) Box plots showing SUV_{max} for ^{18}F-PSMA-1007– and ^{18}F-DCFPyL–positive lesions. *Statistically significant (with *P* value shown on *x*-axis).

and background clearance, which has a relevant impact on the practicability of a particular tracer for routine clinical use. For example, the dimerized form, [Glu-ureido-Lys(Ahx)]$_2$-HBED-CC (HBED-CC is *N,N′*-bis[2-hydroxy-5-(carboxyethyl)benzyl]ethylenediamine-*N,N′*-diacetic acid), named PSMA-10, presented with a higher PSMA binding affinity (half-maximal inhibitory concentration, 3.9 vs. 12.1 nM) than the monomer PSMA-11 (*16*), but because of the capability of early image acquisition, the monomer became the standard tracer for imaging in combination with the short-lived radionuclide ^{68}Ga (*1*). Because of the longer half-life of ^{18}F, delayed imaging is possible using the radiofluorinated compounds. In particular, ^{18}F-PSMA-1007 demonstrated a remarkable increase in SUV when imaging was postponed until 3 h after injection (*8*). In contrast, imaging 2 h after injection was suggested for application of ^{18}F-DCFPyL by various groups (*7,9*). In this study, we decided to image 2 h after injection as a physician's choice in searching for a reasonable trade-off between contrast and optimal patient throughput in clinical practice.

The intraindividual comparisons are reasonable for this small patient population and highlight the potential benefit of each tracer's characteristics for the few patients with individually challenging situations. Larger comparison trials will be needed to validate the hypothesis that ^{18}F-PSMA-1007 might be advantageous for evaluation of the prostatic bed and ^{18}F-DCFPyL in the evaluation of liver metastases. No conclusion can be drawn from this study regarding the diagnostic performance of either tracer in imaging of prostate cancer, as this was not the aim of the study.

CONCLUSION

This study demonstrated that both ^{18}F-DCFPyL and ^{18}F-PSMA-1007 are widely equivalent for imaging of local and metastatic prostate cancer. Both tracers provide excellent image quality. Because evaluation of the pelvis is more frequently the focus of prostate cancer imaging than of liver staging, the nonurinary excretion of ^{18}F-PSMA-1007 presents a theoretic advantage, especially for primary staging and in cases of suspected local recurrence.

DISCLOSURE

Frederik L. Giesel, Klaus Kopka, and Uwe Haberkon are named on a patent application for PSMA-1007. No other potential conflict of interest relevant to this article was reported.

ACKNOWLEDGMENTS

We acknowledge Nuclear Technology Products (NTP), the South African Nuclear Energy Corporation (NECSA), and the Steve Biko Academic Hospital Nuclear Medicine Department for assistance with the radiosyntheses of ^{18}F-PSMA-1007 and ^{18}F-DCFPyL and scanning of patients. We thank Daniel Burkert, Division of Radiopharmaceutical Chemistry, DKFZ Heidelberg, Germany, for technical assistance with the radiosyntheses of ^{18}F-PSMA-1007 and ^{18}F-DCFPyL.

REFERENCES

1. Perera M, Papa N, Christidis D, et al. Sensitivity, specificity, and predictors of positive ^{68}Ga-prostate-specific membrane antigen positron emission tomography in advanced prostate cancer: a systematic review and meta-analysis. *Eur Urol.* 2016;70:926–937.
2. Kratochwil C, Afshar-Oromieh A, Kopka K, Haberkorn U, Giesel FL. Current status of prostate-specific membrane antigen targeting in nuclear medicine: clinical translation of chelator containing prostate-specific membrane antigen ligands into diagnostics and therapy for prostate cancer. *Semin Nucl Med.* 2016;46:405–418.
3. Schwarzenboeck SM, Rauscher I, Bluemel C, et al. PSMA ligands for PET imaging of prostate cancer. *J Nucl Med.* 2017;58:1545–1552.
4. Eiber M, Fendler WP, Rowe SP, et al. Prostate-specific membrane antigen ligands for imaging and therapy. *J Nucl Med.* 2017;58(suppl 2):67S–76S.
5. Chen Y, Pullambhatla M, Foss CA, et al. 2-(3-{1-carboxy-5-[(6-[^{18}F]fluoro-pyridine-3-carbonyl)-amino]-pentyl}-ureido)-pentanedioic acid, [^{18}F]DCFPyL, a PSMA-based PET imaging agent for prostate cancer. *Clin Cancer Res.* 2011; 17:7645–7653.
6. Cardinale J, Schafer M, Benesova M, et al. Preclinical evaluation of ^{18}F-PSMA-1007, a new prostate-specific membrane antigen ligand for prostate cancer imaging. *J Nucl Med.* 2017;58:425–431.
7. Szabo Z, Mena E, Rowe SP, et al. Initial evaluation of [^{18}F]DCFPyL for prostate-specific membrane antigen (PSMA)-targeted PET imaging of prostate cancer. *Mol Imaging Biol.* 2015;17:565–574.
8. Giesel FL, Hadaschik B, Cardinale J, et al. F-18 labelled PSMA-1007: biodistribution, radiation dosimetry and histopathological validation of tumor lesions in prostate cancer patients. *Eur J Nucl Med Mol Imaging.* 2017;44:678–688.
9. Dietlein F, Kobe C, Neubauer S, et al. PSA-stratified performance of ^{18}F- and ^{68}Ga-PSMA PET in patients with biochemical recurrence of prostate cancer. *J Nucl Med.* 2017;58:947–952.
10. Cardinale J, Martin R, Remde Y, et al. Procedures for the GMP-compliant production and quality control of [^{18}F]PSMA-1007: a next generation radiofluorinated tracer for the detection of prostate cancer. *Pharmaceuticals (Basel).* 2017;10:E77.
11. Afshar-Oromieh A, Malcher A, Eder M, et al. PET imaging with a [^{68}Ga]gallium-labelled PSMA ligand for the diagnosis of prostate cancer: biodistribution in humans and first evaluation of tumour lesions. *Eur J Nucl Med Mol Imaging.* 2013;40:486–495.
12. Vallabhajosula S, Nikolopoulou A, Babich JW, et al. ^{99m}Tc-labeled small-molecule inhibitors of prostate-specific membrane antigen: pharmacokinetics and biodistribution studies in healthy subjects and patients with metastatic prostate cancer. *J Nucl Med.* 2014;55:1791–1798.
13. Kopka K, Benesova M, Barinka C, Haberkorn U, Babich J. Glu-ureido-based inhibitors of prostate-specific membrane antigen: lessons learned during the development of a novel class of low-molecular-weight theranostic radiotracers. *J Nucl Med.* 2017;58(suppl):17S–26S.
14. Sanchez-Crespo A. Comparison of gallium-68 and fluorine-18 imaging characteristics in positron emission tomography. *Appl Radiat Isot.* 2013;76:55–62.
15. Goffin KE, Joniau S, Tenke P, et al. Phase 2 study of ^{99m}Tc-trofolastat SPECT/CT to identify and localize prostate cancer in intermediate- and high-risk patients undergoing radical prostatectomy and extended pelvic LN dissection. *J Nucl Med.* 2017;58:1408–1413.
16. Schafer M, Bauder-Wust U, Leotta K, et al. A dimerized urea-based inhibitor of the prostate-specific membrane antigen for ^{68}Ga-PET imaging of prostate cancer. *EJNMMI Res.* 2012;2:23.